



# Antibacterial Properties and Mechanism of Lysozyme-Modified ZnO Nanoparticles

Kangrui Yuan<sup>1†</sup>, Xiaoliu Liu<sup>2†</sup>, Jianxin Shi<sup>1</sup>, Wei Liu<sup>1</sup>, Kun Liu<sup>1</sup>, Hongmei Lu<sup>3</sup>, Dudu Wu<sup>1</sup>, Zhi Chen<sup>1\*</sup> and Chengyu Lu<sup>1\*</sup>

<sup>1</sup>School of Pharmacy, Guangdong Medical University, Dongguan, China, <sup>2</sup>Medical Laboratory of Shenzhen Luohu People's Hospital, Shenzhen, China, <sup>3</sup>The First Dongguan Affiliated Hospital of Guangdong Medical University, Dongguan, China

## OPEN ACCESS

### Edited by:

Lei Wang,  
Harbin Institute of Technology, China

### Reviewed by:

Bin Dong,  
Soochow University, China  
Kelong Fan,  
Institute of Biophysics (CAS), China  
Haixu Chen,  
Harbin Institute of Technology, China

### \*Correspondence:

Zhi Chen  
czwududu@126.com  
Chengyu Lu  
gdmuluchengyu@126.com

<sup>†</sup>These authors have contributed equally to this work and share first authorship

### Specialty section:

This article was submitted to  
Nanoscience,  
a section of the journal  
Frontiers in Chemistry

Received: 21 August 2021

Accepted: 25 October 2021

Published: 26 November 2021

### Citation:

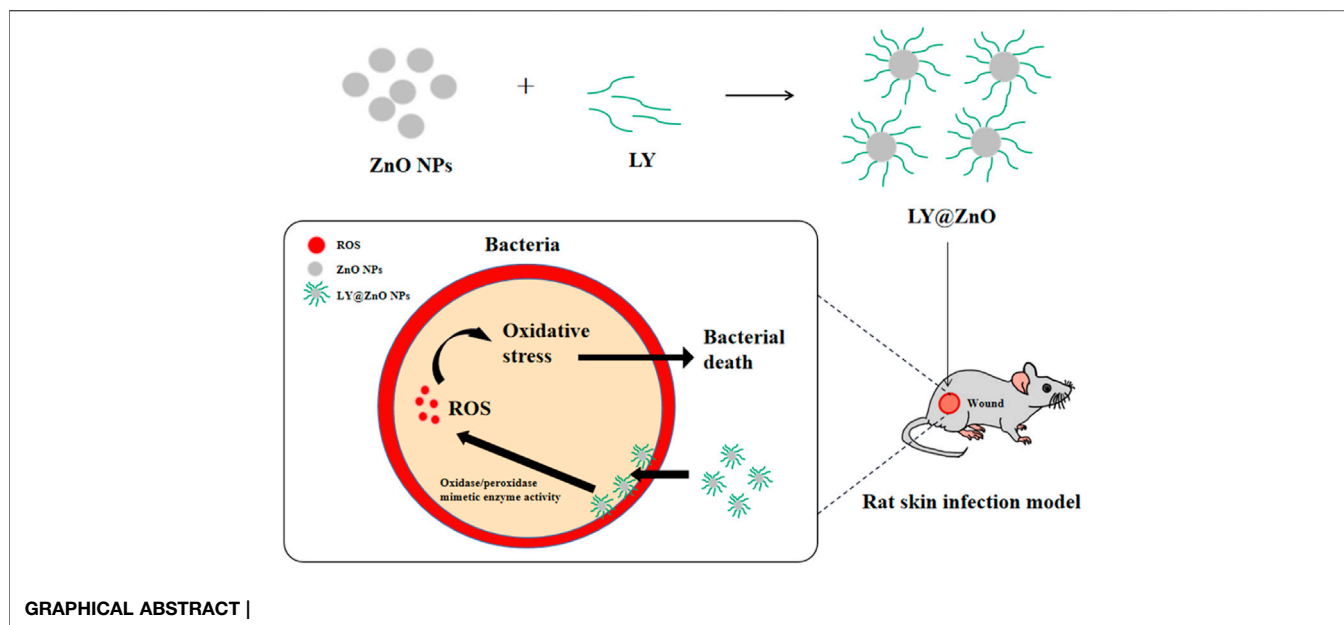
Yuan K, Liu X, Shi J, Liu W, Liu K, Lu H, Wu D, Chen Z and Lu C (2021) Antibacterial Properties and Mechanism of Lysozyme-Modified ZnO Nanoparticles. *Front. Chem.* 9:762255. doi: 10.3389/fchem.2021.762255

The lysozyme-modified nanoparticles (LY@ZnO NPs) were synthesized by the reduction–oxidation method, and the morphology and structure of LY@ZnO were analyzed by Fourier transform infrared (FTIR) spectroscopy, powder X-ray diffraction (XRD), scanning electron microscope (SEM), and particle size analysis. The antibacterial effects of LY@ZnO against *Escherichia coli* (*E. coli*, Gram-negative bacteria) and *Staphylococcus aureus* (*S. aureus*, Gram-positive bacteria) were discussed by measuring the zone of inhibition (ZOI) and growth inhibition. The antimicrobial experiments showed that the LY@ZnO NPs possessed better antibacterial activity than ZnO. Besides, the antibacterial mechanism of LY@ZnO was also investigated, which was attributed to the generation of reactive oxygen species (ROS). Furthermore, the toxicities of LY@ZnO *in vivo* and *in vitro* were discussed by the cell counting kit-8 method and animal experiments, showing that LY@ZnO possessed excellent biocompatibility. Finally, the therapeutic effect of LY@ZnO on a rat skin infection model caused by methicillin-resistant *Staphylococcus aureus* (MRSA) was also studied, which exhibited good anti-infective activity. Our findings showed that LY@ZnO possessed remarkable antibacterial ability due to its excellent membrane permeability and small particle size. Besides, LY@ZnO also exhibited certain stability and great safety, which showed tremendous prospects for microbial infection in patients. It would also be helpful for a better understanding of the enzyme-modified nanomaterials against bacteria.

**Keywords:** enzyme, lysozyme, ZnO nanoparticles, nanomaterials, antibacterial activity

## INTRODUCTION

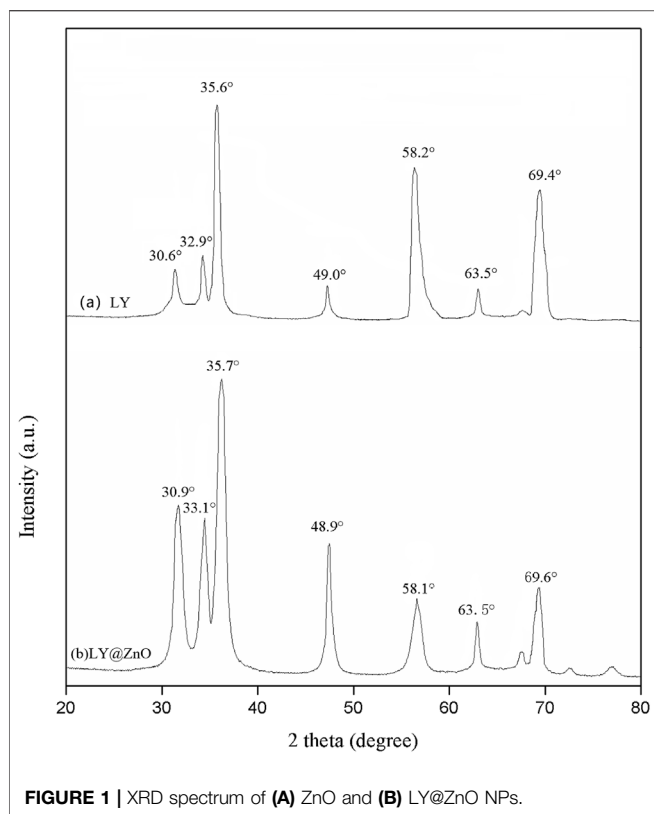
Bacterial infections have always been the main threat to human health all over the world (Deusenbery et al., 2021). According to the statistics from the World Health Organization (WHO), bacterial infections have been the leading cause of death in developing countries for the past decades (Eyvazi et al., 2020). However, the antibiotic-resistant bacteria (ARB) that are developed due to antibiotic drug abuse have significantly threatened public health. The production of ARB (especially superbug) has affected the therapeutic effect of traditional antibiotics (Theuretzbacher et al., 2020). So, researchers are dedicated to discover new drugs which can adequately inhibit bacterial growth and kill bacteria.



In the past decades, nanomaterials have achieved remarkable success in energy, catalysis, analysis, imaging, and diseases (Gao et al., 2004; Guo and Wang, 2011; Silvestre et al., 2011; Zhou et al., 2011; Jiang et al., 2012; Biju, 2013; Wang et al., 2020a; Rasal et al., 2021), particularly in the field of antibacterials (Xin et al., 2018). For example, inorganic nanomaterials (such as metal oxides) have attracted much attention due to their outstanding safety, stability, bio-distribution, and clearance (Chen et al., 2016; Guo et al., 2020; Wang et al., 2021a). Moreover, nanomaterials exhibited higher membrane permeability, which led to remarkable antibacterial ability, especially toward ARB (Han et al., 2017). Some literature reported that the nanomaterials could perform multiple bactericidal pathways, making it difficult for bacteria to adapt to these treatments, with great properties against ARB (Hajipour et al., 2012). Zinc oxide (ZnO, an essential metal oxide antibacterial) has aroused lots of attention because of its stability, bio-compatibility, and fast electron transfer kinetics (Du et al., 2021). Besides, ZnO NPs can damage the bacteria by the generation of the ROS, while the release of Zn ions leads to the dysfunction of critical components (such as DNA) (Qi et al., 2017). Hence, several studies on the antimicrobial properties of ZnO NPs are reported. For instance, Jian et al. investigated Ag nanoparticle-decorated ZnO nanorod arrays, which showed significantly high antibacterial properties against *Pseudomonas aeruginosa* (Shang et al., 2019, 2020). Lan et al. found that the ZnO nanorods modified by the CeO<sub>2</sub> NPs possessed antimicrobial capability toward the selected bacteria (*E. coli* and *S. aureus*) (Lan et al., 2018). Gutha et al. synthesized a CS-ZnO-based hybrid antibacterial material that displayed significant antibacterial effects against *E. coli* and *S. aureus*, while the antimicrobial rate has reached 99% in 3 h (Gutha et al., 2017). However, the cytotoxicity and poor

selectivity limited the application of nanomaterials as antibacterial agents. Therefore, to improve the biocompatibility of nano antibacterial agents has become a major need in this field.

Besides, enzymes are used as antibacterial agents due to the high selectivity toward substrates and high reaction efficiency under mild reaction conditions (Wang et al., 2019a; Wang et al., 2019b; Wang et al., 2020b; Mei et al., 2021; Tang et al., 2021; Wei et al., 2021; Zhang et al., 2021; Zhao et al., 2021). Lysozyme (LY), a typical antibacterial hydrolase, has attracted many interests due to its non-toxicity, specificity to hydrolyze towards bacterial walls, and the enhancement of immunity (Wu et al., 2017). For example, Ye et al. prepared hydrogel-immobilized lysozyme as an antibacterial agent, showing inhibition efficiency as high as 99.4% (against *E. coli* and *B. subtilis*) and a high effective duration of up to 55 days (Ye et al., 2019). Xiao et al. invented a moisture balanced antibacterial dressing loaded with lysozyme, which could facilitate the wound of infected mice healing, proving the lysozyme dressing could prevent infection of bacteria, efficiently (Xiao et al., 2019). Wu et al. reported that the lysozyme could cure the otorhinolaryngological inflammatory diseases (such as acute pharyngitis, acute laryngitis, and acute otitis media) caused by bacterial infection, effectively (Wu et al., 2017). However, the application of the lysozyme is limited by its unstable structure. Therefore, the design of a novel nano antibacterial agent to improve the antibacterial activity, stability, and biocompatibility was a promising research. In this research, ZnO nano antibacterial agents modified by the lysozyme displayed the following advantages: 1) the usage of lysozyme to modify ZnO could improve the selectivity and safety of the nanomaterials; 2) the utilization of ZnO as nanocarriers could improve the stability to acid and heat of enzyme due to the inherent core material, shape, size, and surface chemistry of



nanomaterial; and 3) ZnO nanoparticles modified by lysozyme could exhibit the synergistic antibacterial effects.

Moreover, available research demonstrated that the ZnO antimicrobial agents could present their antibacterial effects by the production of intracellular ROS (Aničić et al., 2018; De Meutter and Goormaghtigh, 2020). For example, Traian et al. investigated the Mn-doped ZnO nanoparticles, which could promote the intracellular reactive oxygen species (ROS) generation in NIH3T3 fibroblast cells (Popescu et al., 2020). Bikram et al. studied the controlled copper doping in ZnO nanoparticles, finding that the nanoparticles could elicit ROS generation in macrophages (Das et al., 2019). Furthermore, the ROS-induced antimicrobial activity of metallic nanomaterials is often related to their intrinsic oxidase and peroxidase-mimetic enzyme catalytic activity (Yin et al., 2016; Chen et al., 2018). Many nanomaterials could produce ROS via the activities of oxidase-mimetic enzyme and peroxidase-mimetic enzyme.

In this study, the ZnO NPs modified with the lysozyme were successfully synthesized, and the structure of LY@ZnO was investigated by FTIR, XRD, SEM, and particle size analysis. Then, the antibacterial effects of LY@ZnO (enzyme-modified nanoantibiotics) against *E. coli* and *S. aureus* were studied via the turbidimetric method and disk-diffusion methods and found that compared with other common antibacterial agents, LY@ZnO possessed a remarkably good antibacterial effect. Besides, LY@ZnO also displayed low toxicities toward normal cells after a series of cytotoxicity assays, while showing no harm to rat organs in tissue section experiments. Furthermore, the antibacterial

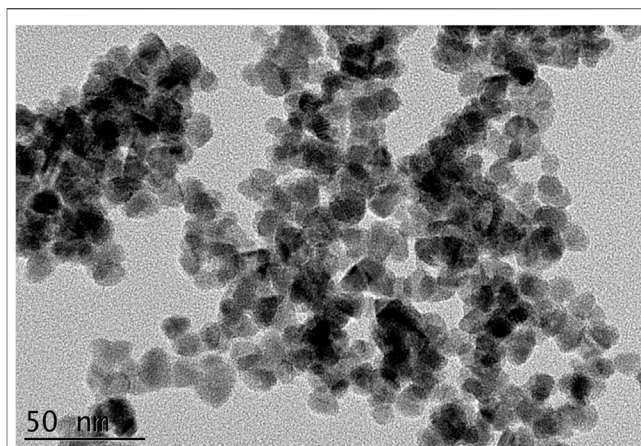
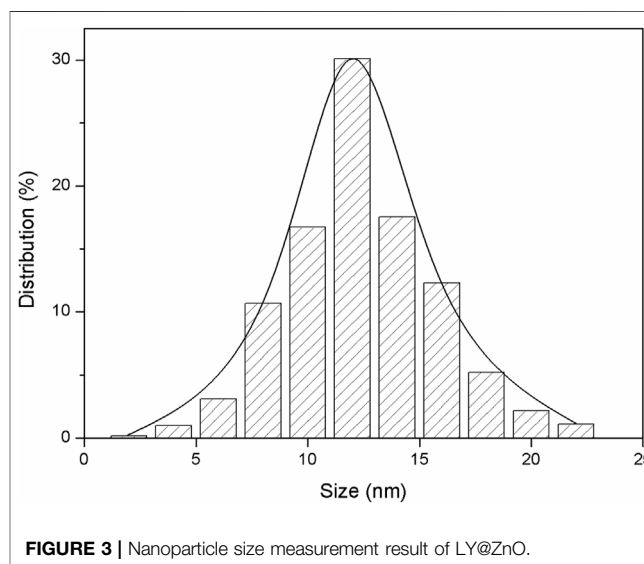


**FIGURE 2** | SEM image of LY@ZnO NPs.

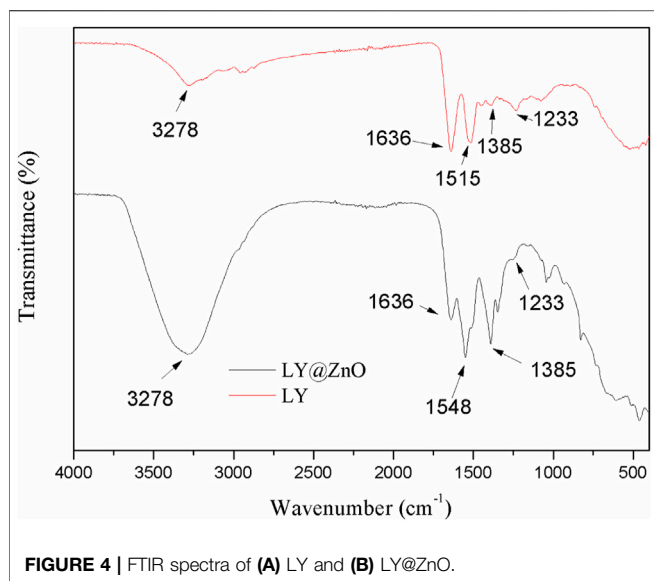


ability of LY@ZnO *in vivo* was discussed by the rat trauma infection model. Finally, the antibacterial mechanism of LY@ZnO NPs against *E. coli* and *S. aureus* was also investigated.

## MATERIALS AND METHODS

### Materials and Reagents

2',7'-dichlorofluorescein diacetate (DCFHDA) and zinc nitrate hexahydrate [ $\text{Zn}(\text{NO}_3)_2 \cdot 6\text{H}_2\text{O}$ ] were bought from Shanghai Solarbio Co. Ltd. N-acetylcysteine (NAC) was obtained from Guangdong Macklin Biochemical Co. Ltd. LB agar powder and Reactive Oxygen Species Assay Kit were obtained through Dongguan Sigma-Aldrich. Gentamycin was bought from Guangzhou Macklin Co. Ltd. Yeast extract and tryptone were obtained from Shenzhen Macklin Biochemical Co. Ltd. Lysozyme was obtained from English Oxoid Corporation, and the sodium chlorides (NaCl) were bought from Shenzhen Solarbio Science



and Technology Co. Ltd. *E. coli* (ATCC52922) and *S. aureus* (ATCC25923) were obtained from Zhanjiang Damao Co. Ltd. In this study, all chemical reagents were used at analytical grade, meaning that the reagents cannot be purified further.

The images of LY@ZnO were captured by Japan JEOL JEM-2100 Transmission Electron Microscope. The fluorescence spectroscopy was recorded by Japan Shimadzu RF-5301PC. The ultraviolet spectroscopy was studied by Thermo Fisher. The absorbance was obtained by Thermo Fisher's Biomate 3S enzymatic labels. Zeta potential was measured by Nano ZS Zetasizer 90.

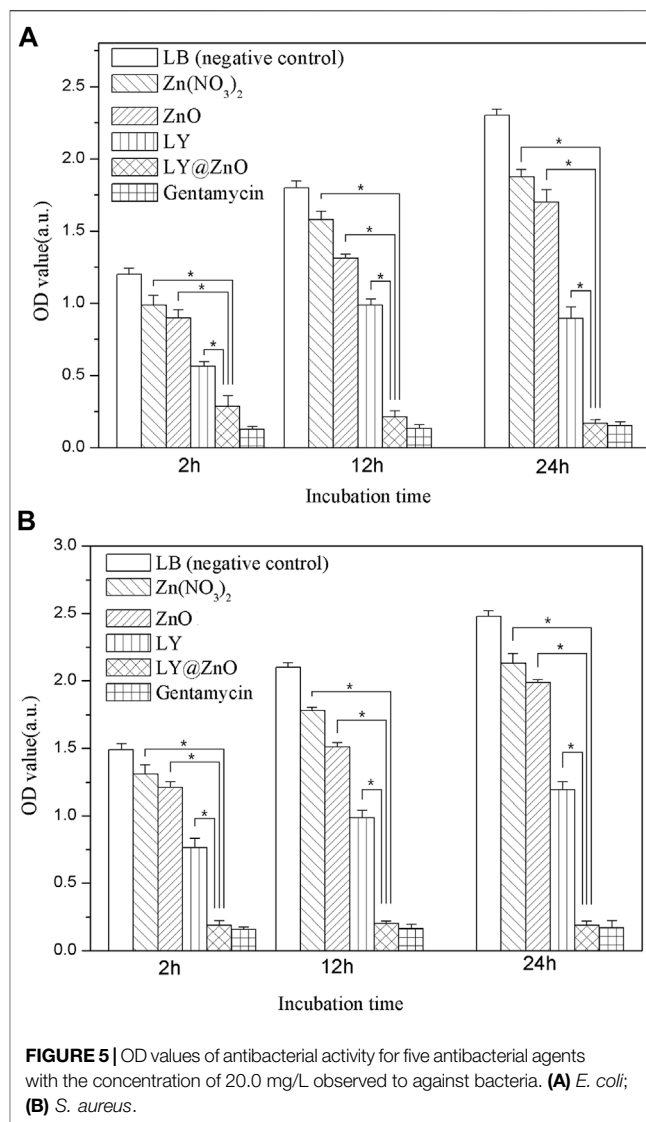
## Synthesis of LY@ZnO

The LY@ZnO NPs were obtained via the oxidation–reduction method (Cao et al., 2011). First, 50 ml LY solution ( $5.0 \times 10^{-5}$  mol/L) was mixed with 50 ml  $Zn(NO_3)_2$  ( $7.5 \times 10^{-2}$  mol/L) in a 100-ml flask. The mixture was maintained for 24 h for the formation of the solution with LY- $Zn^{2+}$  complexes. Then, 25 ml  $NaBH_4$  (0.10 mol/L) was added into the flask with vigorous stirring. Besides, the solution was kept under room temperature for 12 h with the protection of  $N_2$ . Afterward, the samples would be separated *via* centrifugation at 10,000 rpm for 10 min. The collected samples were washed by anhydrous ethanol and vacuum dried for 24 h. Finally, the samples were calcinated under  $80^\circ C$  for 6 h. The LY-conjugated ZnO NPs (white powders) were gained.

## Antibacterial Experiment

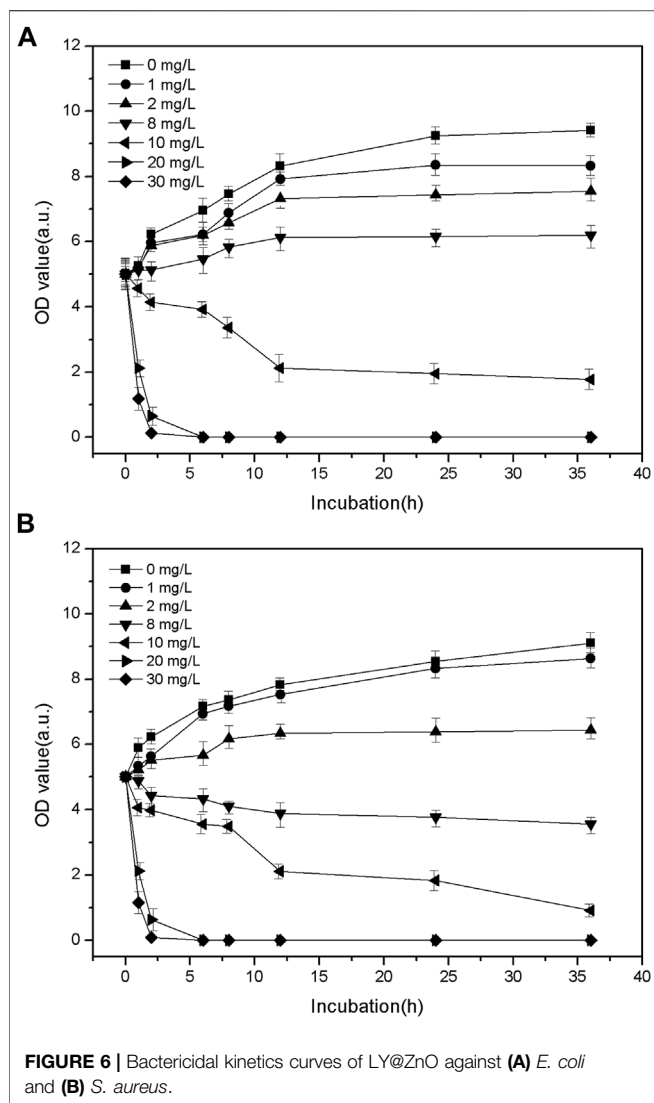
### Evaluation of Antibacterial Activity

The antibacterial ability of LY@ZnO was studied against two common clinical bacteria (*E. coli* and *S. aureus*) by turbidimetric method, while the minimal inhibitory concentration (MIC) of LY@ZnO was revealed. The LB medium was made of 10 g/L sodium chloride, 5 g/L yeast extract, and 10 g/L tryptone. Besides,  $1.0 \times 10^7$  CFU/ml of bacterial suspensions were inoculated into 2 ml of LB medium



(additionally containing 20 mg/L of  $Zn(NO_3)_2$ , ZnO NPs, LY, and LY@ZnO). Then, the antibacterial efficacy would be calculated by directing the measurement of scattered light from samples.

The inhibition zone of the samples [ $Zn(NO_3)_2$ , ZnO NPs, LY, LY@ZnO, and gentamycin] were tested by the disk diffusion method, which indicated the antibacterial efficiency of the samples to be tested. First, 20 ml of LB medium was poured onto the sterilized plates until it solidifies horizontally. Then, the 0.1 ml strains were injected on the LB medium, which was coated. In addition, the filter planes with 15  $\mu L$  respective sample solutions were added on the agar plate. The plates permeated with the equivalent LB liquids were regarded as the negative control. The dishes would be cultured at  $37^\circ C$  for 12 h, and the diameter of ZOI was measured. All experiments were duplicated three times under the same conditions.



### Bactericidal Kinetics

To further evaluate the antibacterial activity of LY@ZnO, the time–disinfection kinetic curve was investigated under LY@ZnO treatment at different time points. The bacterial suspension ( $1.0 \times 10^5$  CFU/ml) should be added into the different concentrations of LY@ZnO, which would be calculated with an oscillator at  $37^\circ\text{C}$  for 24 h. Then, 100  $\mu\text{L}$  samples were diluted and coated on the LB medium, while the bacteria cultured for 0, 1, 3, 6, 12, 18, and 24 h would be gathered, respectively. The number of colonies was counted after the collected bacteria were cultured for 24 h.

### Measurement of ROS

The ROS within the bacteria was tested via the Reactive Oxygen Species Assay Kit from Beyotime (Pinegin et al., 2017). First,  $1.0 \times 10^8$  CFU/ml of bacteria mixed with LY@ZnO would be centrifuged and gathered after culturing for 2 h at  $37^\circ\text{C}$ . After being washed with sterile water three times, the sample would be processed by 2',7'-dichlorofluorescein diacetate after light-protection incubation for 3 h under room temperature. Then,

the fluorescence intensity was measured by the Shimadzu RF-5301 PC Fluorescence Spectrophotometer, while the excitation wavelength was 488 nm and emission wavelength was 525 nm, respectively.

### Activity of Oxidase Mimetic Enzymes

To evaluate the activity of oxidase mimetic enzymes, LY@ZnO was added into  $\text{H}_2\text{O}_2$  from the Hydrogen Peroxide Assay Kit. The concentration of  $\text{H}_2\text{O}_2$  would be measured according to the formula  $c = A/(\epsilon \times b)$  ( $c$ : concentration,  $A$ : absorbance,  $\epsilon$ : molar extinction coefficient,  $b$ : light course). In this experiment, the absorbance was tested by NanoDrop 2000C ( $\epsilon = 43.6 \text{ M}^{-1} \text{ cm}^{-1}$ ,  $b = 1 \text{ cm}$ ). The specific assay procedure should follow the instructions of the kit.

### Activity of the Peroxidase-Mimicking Enzyme

To evaluate the activity of the oxidase mimetic enzymes, mixed solutions (containing 20  $\mu\text{L}$  100 mM of 3, 3', 5, 5'-tetramethylbenzidine and 4  $\mu\text{L}$  10 M of  $\text{H}_2\text{O}_2$ ) were added into 2 ml of LY@ZnO. Then, the absorbance was tested by the NanoDrop 2000C at different time points under different concentrations of LY@ZnO.

### Cytotoxicity

#### Toxicity Toward Cells

To evaluate the cytotoxicity of LY@ZnO toward mammalian cells, the viability of the cells (human normal hepatocytes: LO2, human normal lung epithelial cells: BEAS-2B, mouse neural cells: CATH.a, rat cardiomyocytes: H9C2, and rhinoceros fetal kidney cells: MA104) was revealed using the Cell Counting Kit-8 methods (CCK8). All cells were purchased from the Wuhan Procell Life Science and Technology Co., Ltd., which were cultured at  $37^\circ\text{C}$  with 5%  $\text{CO}_2$  in DMEM, which was complemented with 10% FBS. The LO2, BEAS-2B, CATH.a, H9C2, and MA104 cells were inoculated with 100  $\mu\text{L}$  per well in 96-well plates at a density of  $1 \times 10^4$  cells/mL, respectively, while the 96-well plates would be cultured under 5%  $\text{CO}_2$  at  $37^\circ\text{C}$  for 12 h. Then, 200  $\mu\text{L}$  DMEM (containing 10% FBS and 0, 5, 10, and 20 mg/L of LY@ZnO) was added into each well for 24 h after washing with PBS for 3 times, and five parallel groups should be set up for each concentration gradient. Afterward, 10  $\mu\text{L}$  CCK8 was put into the well and then cultured at  $37^\circ\text{C}$  with 5%  $\text{CO}_2$  for 2 h. The UV absorption intensity of 96-well plates was measured by an enzyme marker at 450 nm. Cell survival rate (%) =  $[(\text{As} - \text{Ab}) / (\text{Ac} - \text{Ab})] \times 100\%$  ( $\text{As}$ : experiential wells,  $\text{Ab}$ : blank wells with DMEM but no cells,  $\text{Ac}$ : control wells with cells but no LY@ZnO).

#### Tissue Section Observation

The 4-week-old SD female rats were purchased from the Guangdong Animal Centre, while the breeding of the rats and the animal experiments were processed in the Guangdong Medical University Laboratory Animal Centre. The 200  $\mu\text{L}$  20 mg/L of LY@ZnO was intraperitoneally injected into the rats, while the sanitary saline was regarded as the control group. The heart, liver, spleen, lungs, and kidneys of rats would be extracted after processing, which was immersed in 4% formalin. The sample would be stained by hematoxylin–eosin

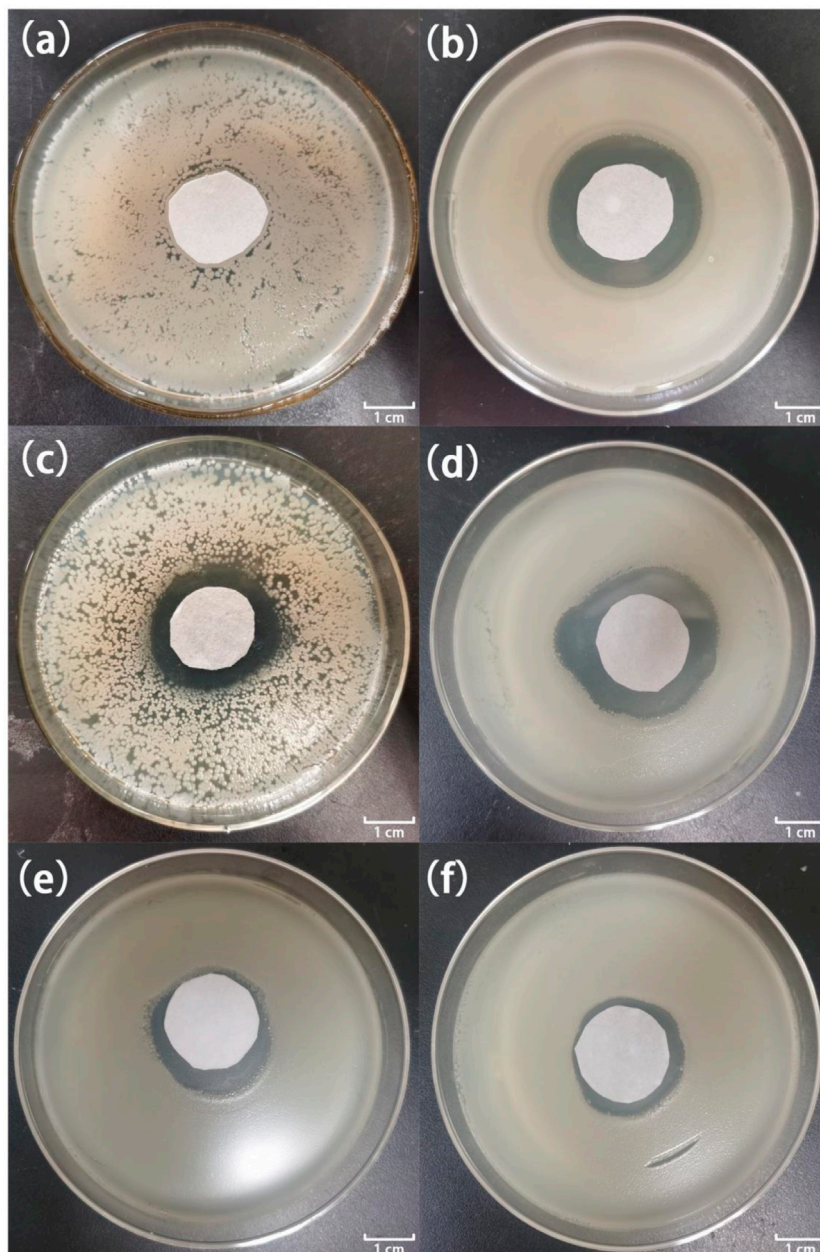


**FIGURE 7** | Images of inhibition zones for different samples against *E. coli*. **(A)** 0.0 µg; **(B)** 20.0 µg gentamycin; **(C)** 5.0 µg LY@ZnO; **(D)** 20.0 µg LY@ZnO; **(E)** 20.0 µg LY; and **(F)** 20.0 µg ZnO.

staining method after the paraffin section. Then, the slices were observed under an optical microscope.

### Rat Infection Model

To investigate the antibacterial ability of LY@ZnO *in vivo*, 200 µL  $1.0 \times 10^9$  CFU/ml of MRSA was subcutaneously injected on the wounds of the infected rats. The 100 µL 10 mg/L of LY@ZnO was injected into rats by intraperitoneal injection, while the 100 µL of sanitary saline was used as the negative group and the 100 µL 10 mg/L gentamycin was used as the positive group. The size of

the wounds was measured after 10 d of treatment. The bacteria were collected from the wounds, cultured in the LB medium, and the OD values were detected by the turbidimetric method.

## RESULTS

### Characterization of LY@ZnO

**Figure 1** shows the XRD spectrum of ZnO and LY@ZnO (LY-modified ZnO NPs). The characteristic diffraction peaks of  $30.9^\circ$ ,

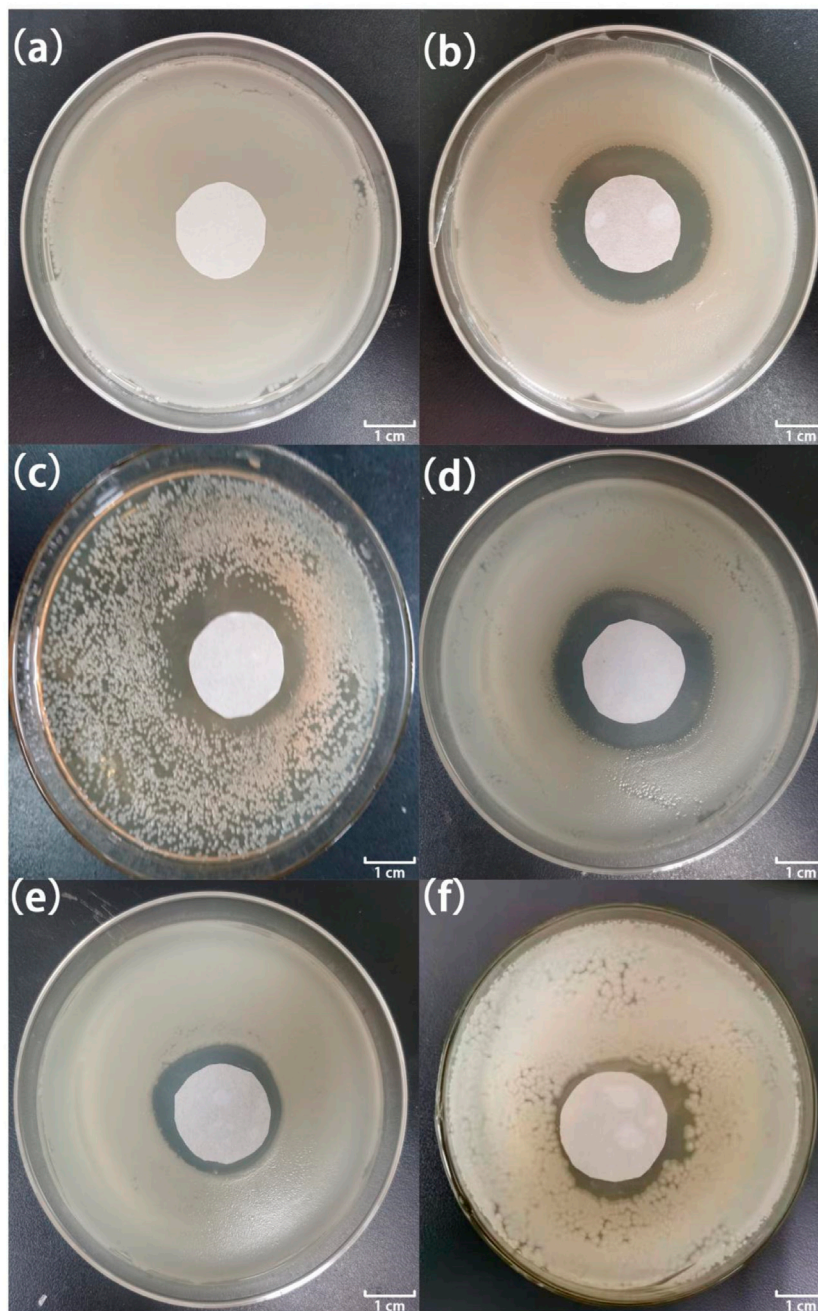


**FIGURE 8** | Images of inhibition zones for different samples against *S. aureus*. **(A)** 0.0 µg; **(B)** 20.0 µg gentamycin; **(C)** 5.0 µg LY@ZnO; **(D)** 20.0 µg LY@ZnO; **(E)** 20.0 µg LY; and **(F)** 20.0 µg ZnO.

33.1°, 35.7°, 48.9°, 58.1°, 63.5°, and 69.6° were found to be the typical (100), (002), (101), (102), (110), (103), and (112) crystal peaks of ZnO NPs, respectively (JCPDS card: 36-1451). Besides, the crystal size ( $D$ ) of LY@ZnO could be calculated by the Scherrer's equation:  $D = k (\lambda/\beta \cos \theta)$  ( $k = 0.89$ , which is a constant;  $\lambda = 0.154$  nm, which is the wavelength of the X-ray;  $\beta$  is the full width at half maximum; and  $\theta = 27.2^\circ$ , which is the half

diffraction angle), and the average sizes ( $D$ ) were calculated to be 11 nm.

The TEM image of the LY@ZnO is presented in **Figure 2**. The NPs were the regular circles, and the average diameter was 12 nm (standard deviation values are calculated to be 1.09 from 10 samples). **Figure 3** shows the nanoparticle dimensions of LY@ZnO tested by the nanoparticle size analyzer, and the nano size of

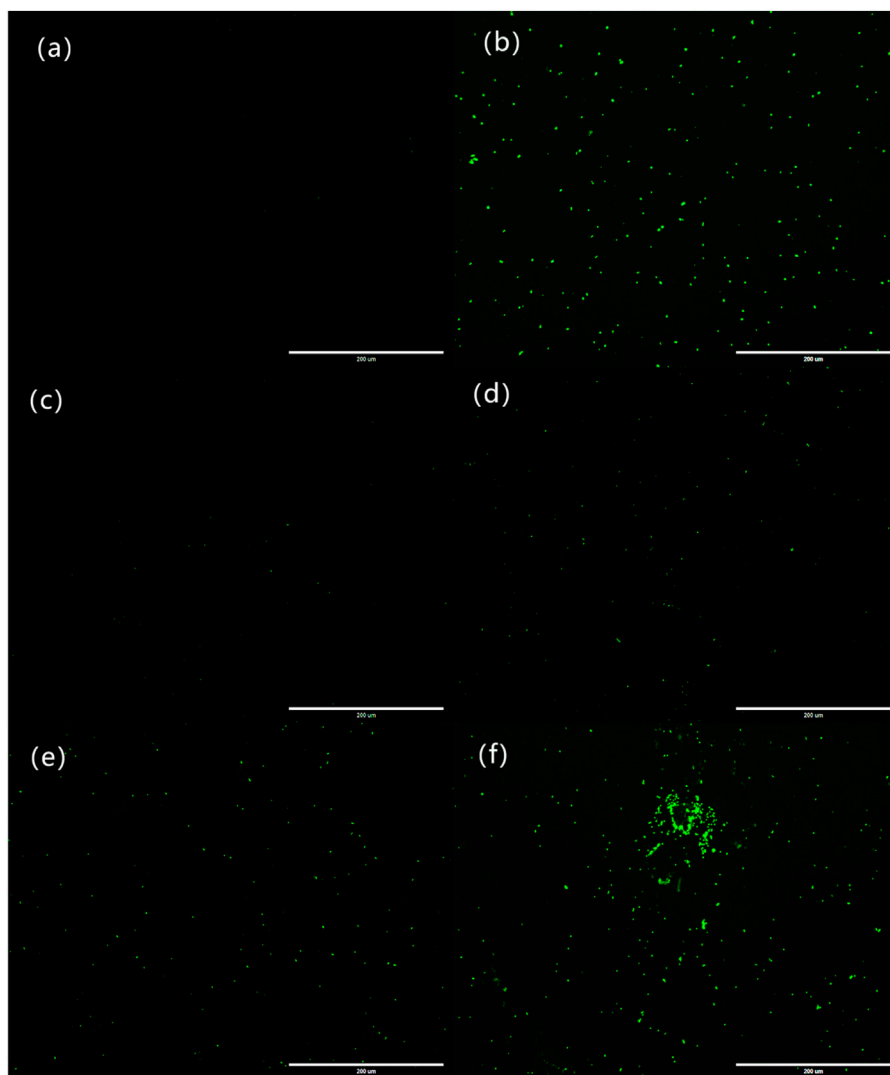


**FIGURE 9** | Laser confocal microscopy to observe the effect of LY@ZnO on ROS in bacteria. **(A)** 0.0 mg/L LY@ZnO; **(B)** 20.0 mg/L gentamycin; **(C)** 20.0 mg/L LY; **(D)** 20.0 mg/L ZnO; **(E)** 5.0 mg/L LY@ZnO; and **(F)** 20.0 mg/L LY@ZnO.

LY@ZnO was determined to be about 12 nm. Therefore, the sizes of the LY@ZnO detected from the nanoparticle size analyzer were consistent with the TEM image and XRD analysis.

As shown in **Figure 4**, the LY and LY@ZnO NPs were analyzed via FTIR spectroscopy. The bands at  $1,636\text{ cm}^{-1}$ ,  $1,515\text{ cm}^{-1}$ ,  $1,385\text{ cm}^{-1}$ , and  $1,233\text{ cm}^{-1}$  were found in the spectra of the LY (shown in **Figure 4A**). The peak at  $1,636\text{ cm}^{-1}$  was generated from the C=O stretching vibration from the carboxyl group; the peak at  $1,515\text{ cm}^{-1}$  was attributed to the N-H bending vibration in the amino group; the peak at  $1,385\text{ cm}^{-1}$  was generated from the C-N stretching vibration in the amino group; the peak at  $1,233\text{ cm}^{-1}$  was attributed to the C-S bending vibration in the sulfhydryl group (De Meutter and Goormaghtigh, 2020). After LY was conjugated with ZnO NPs, the absorption peaks of LY (the peaks at  $1,636\text{ cm}^{-1}$ ,  $1,385\text{ cm}^{-1}$ , and  $1,233\text{ cm}^{-1}$ ) were observed in the FTIR of

LY@ZnO, which indicated that the structural integrity and functional groups of LY had been maintained during the modification process. Besides, the peaks at  $1,515\text{ cm}^{-1}$  were shifted to  $1520\text{ cm}^{-1}$  in the spectra of LY@ZnO compared with the FTIR spectra of LY, suggesting that LY was connected to ZnO via the strong interaction with the amino group of lysozymes.

### Antibacterial Activity

The antibacterial ability of LY@ZnO toward *E. coli* and *S. aureus* is revealed via the turbidimetric method (see in **Figure 5**). The results showed that the OD values (*E. coli* and *S. aureus*) were increased fast when the bacteria was cultured with LB medium (negative group), meaning that the negative group did not possess any inhibition against bacteria. In contrast, OD values were increased slowly when the bacteria were cultured in the

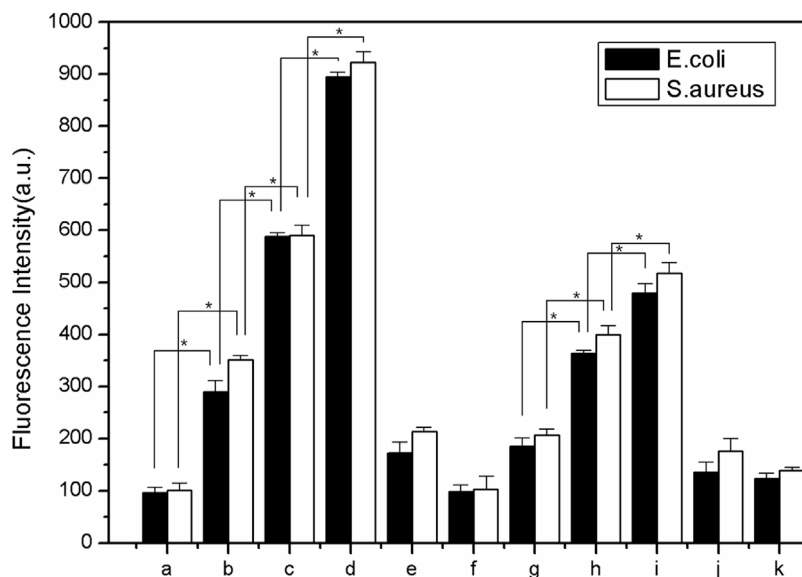


**FIGURE 10** | The qualitative measurement to determine the effect of antioxidant on ROS generation in *E. coli* and *S. aureus* during 24 h (A) 0.0 mg/L LY@ZnO; (B) 5.0 mg/L LY@ZnO; (C) 10.0 mg/L LY@ZnO; (D) 20.0 mg/L LY@ZnO; (E) 20.0 mg/L ZnO (F) 20.0 mg/L LY (G) 10.0  $\mu$ g/L NAC + 20.0 mg/L LY@ZnO (H) 10.0  $\mu$ g/L NAC + 20.0 mg/L LY; and (I) 10.0  $\mu$ g/L NAC + 20.0 mg/L LY@ZnO (J) 10.0  $\mu$ g/L NAC + 20.0 mg/L ZnO.

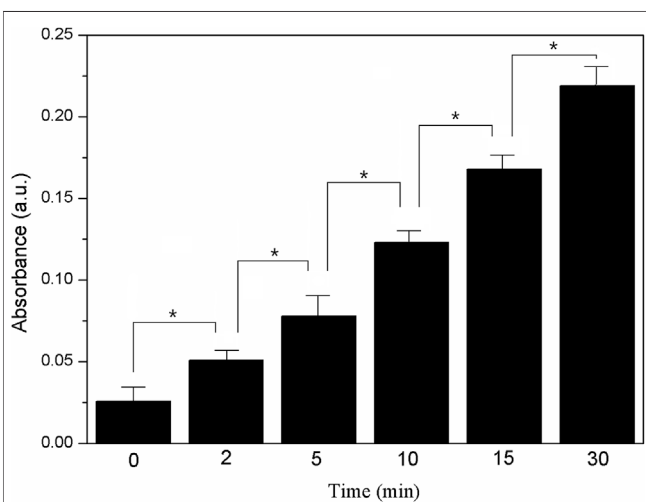


**FIGURE 11** | UV spectra of LY@ZnO mixed with TMB at different times.

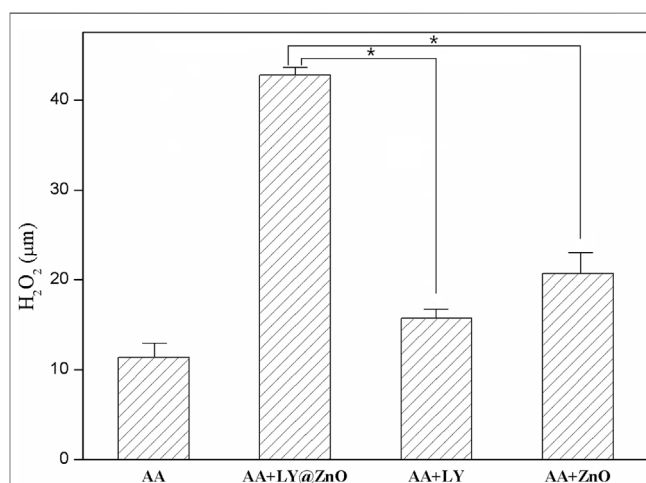
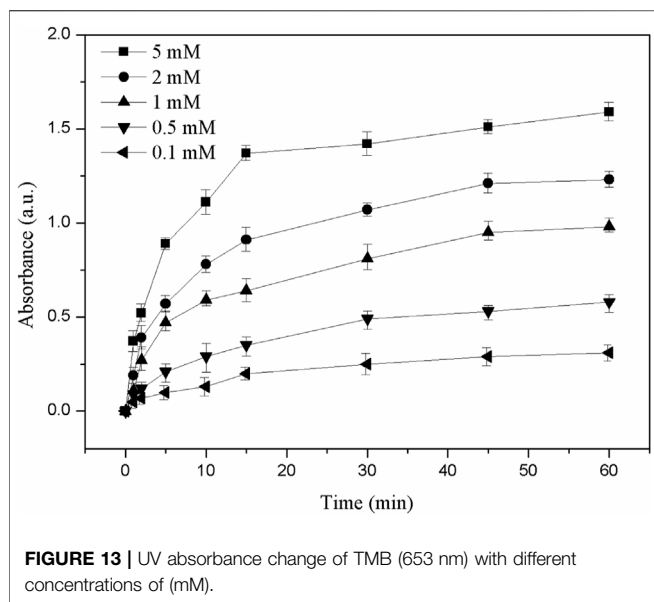


**FIGURE 12** | Concentration of  $H_2O_2$  after treated with AA, AA + LY@ZnO, AA + LY, and AA + ZnO.

positive group (gentamicin), meaning that gentamicin showed significantly good antimicrobial agents. Moreover, the OD values of LY@ZnO were slightly higher than the positive group, indicating that the antibacterial effects of LY@ZnO against microorganisms were prominent. Besides, the OD values of LY and ZnO were higher than those of the LY@ZnO group, suggesting that the ZnO NPs and the LY possessed a certain level of antibacterial effects. These results revealed that LY@ZnO was an outstanding antibacterial agent, and the antibacterial ability might be generated by the collaborative therapeutic effects of LY and ZnO.

The bactericidal kinetics characteristics of LY@ZnO are shown in Figure 6. The OD values were still increased when the bacteria was incubated with a low concentration of LY@ZnO (below 8.0 mg/L). However, the OD values decreased remarkably when the bacteria were cultured with high concentration of LY@ZnO, showing that the high concentration of LY@ZnO could kill both *E. coli* and *S. aureus* effectively. Furthermore, it was found that the OD values were nearly unchanged after 12-h incubation with LY@ZnO, which illustrated that the LY@ZnO NPs could completely inhibit the growth of *E. coli* and *S. aureus*.



after 12 h. The relatively rapid bactericidal kinetic profile further demonstrated its great potential as a nanoantibiotic.

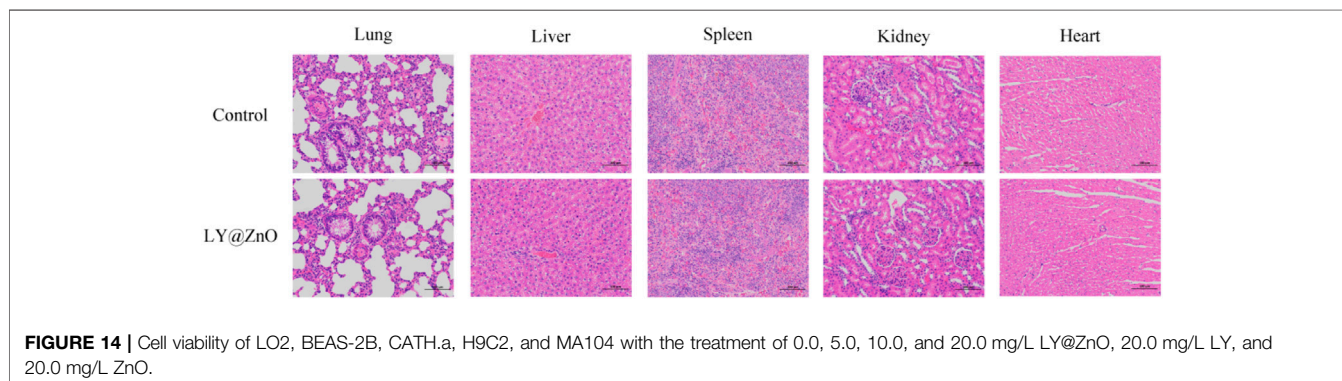
**Figures 7, 8** show the antibacterial effects of LY@ZnO against *E. coli* and *S. aureus* via disc diffusion methods. From the results shown in **Figures 7A, 8A**, we can observe that the negative groups displayed no ZOI, which indicated that the bacteria bred rapidly in the LB medium. Furthermore, the LY and ZnO groups showed small ZOI, exhibiting a certain level of antibacterial ability. Noticeably, as shown in **Figures 7C,D, 8C,D**, the ZOI expanded as the concentration of LY@ZnO increased, meaning that the inhibition of LY@ZnO was dependent on concentrations. Especially, as shown in **Figures 7B,D, 8B,D**, the diameter with high concentrations was almost the same as the diameter of the positive group (*E. coli* and *S. aureus*), which were consistent with the results of the turbidimetric method.

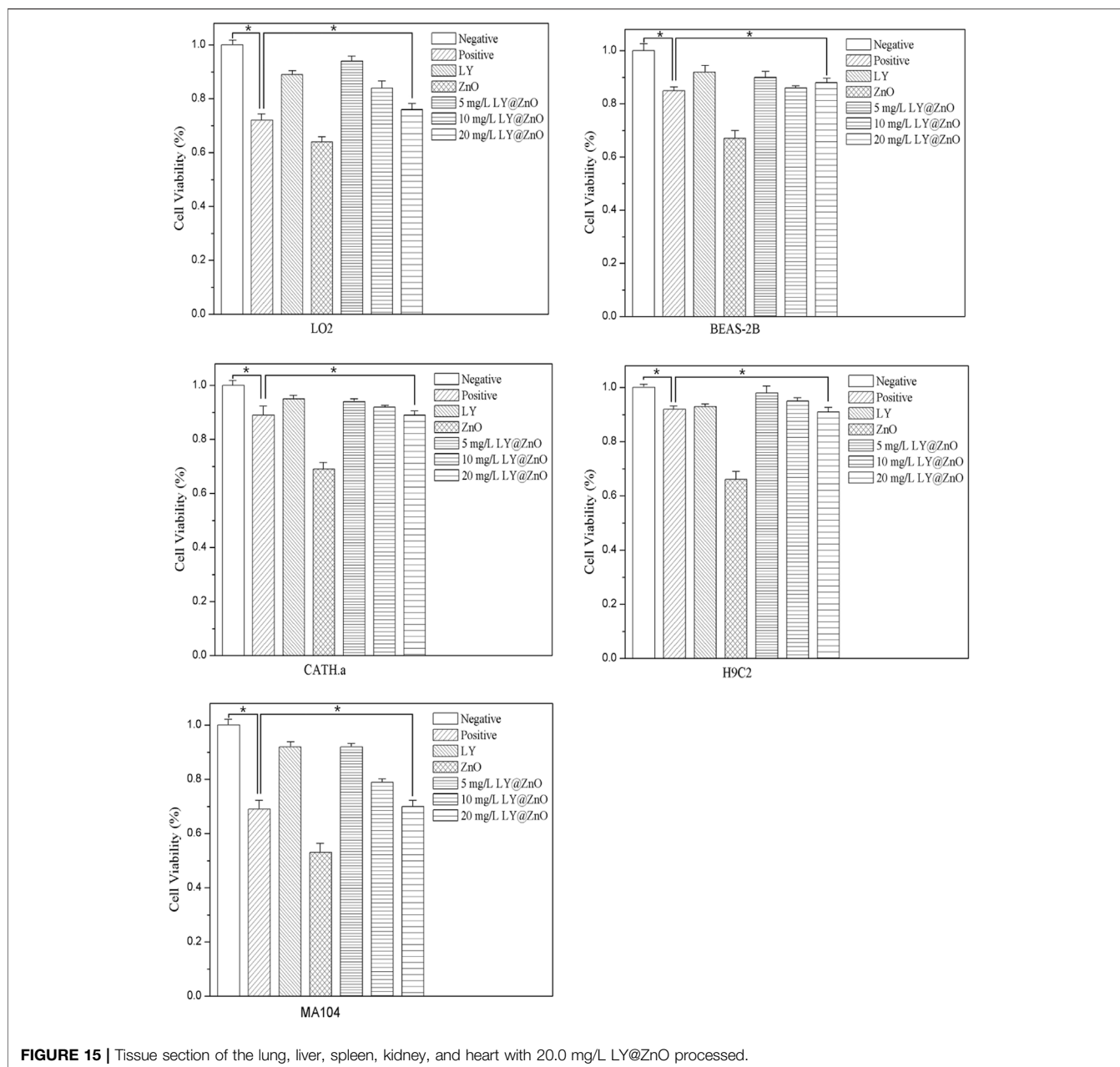
Moreover, the MICs of LY@ZnO against *E. coli*, *S. aureus*, *Streptococcus haemolyticus*, *Corynebacterium diphtheriae*, and *Legionella* were 2.0, 4.0, 8.0, 16.0, and 16.0  $\mu\text{g/ml}$ , respectively. These results suggested that LY@ZnO was an excellent broad-spectrum antimicrobial agent.

## Antibacterial Mechanism ROS Generation

The fluorescence images of the bacterial ROS changes are presented in **Figure 9**, while the production of ROS is presented through the qualitative assessment of LY@ZnO in **Figure 10**. It can be found in **Figure 9** that the fluorescence intensities turned stronger as the concentration of LY@ZnO increased, and these images suggested that the ROS generation was promoted when the LY@ZnO was presented. As shown in **Figure 10A**, the low level of fluorescence intensities belonged to the negative group (only bacteria exist). However, after being treated with LY@ZnO, the fluorescence intensities of *E. coli* and *S. aureus* were higher than those of the negative group, LY group, and ZnO group (see in **Figures 10A,D–F**), showing that more production of ROS resulted from the LY@ZnO group. Furthermore, in the presence of N-acetylcysteine (NAC), the antibacterial effects were also studied. NAC (an effective antioxidant) could prevent the oxidative damage due to the mercapto group of NAC. The fluorescence intensities were remarkably decreased when the NAC was added into 5.0, 10.0, and 20.0 mg/L of LY@ZnO, respectively (see in **Figures 10G–I**). These results clearly illustrated that the antimicrobial activities of LY@ZnO were decreasing in the presence of antioxidants and further explained that the intracellular ROS generation participated in the antibacterial process of LY@ZnO.

Furthermore, it was known that the ROS-induced antimicrobial activity of precious metal nanomaterials was associated with their intrinsic oxidase and peroxidase-mimetic enzymatic catalytic activities (Tao et al., 2014; Aničić et al., 2018; Wang et al., 2021b). The oxidase-mimetic enzymatic activity of LY@ZnO was measured using TMB as a substrate. TMB appeared blue after oxidation and had a maximum UV absorption at 653 nm. As shown in **Figure 11**, the absorbance was increased since LY@ZnO mixed with TMB, indicating that that catalytic reaction started after the TMB mixed with LY@ZnO, and the catalytic efficiency was increased as the reaction time increased. **Figure 12** showed the  $\text{H}_2\text{O}_2$  concentration after being treated with ascorbic acid (common intracellular antioxidants, AA), AA + LY, AA + ZnO, and AA + LY@ZnO, respectively. After  $\text{H}_2\text{O}_2$  was treated with AA, LY, ZnO, and LY@ZnO groups, the concentrations of  $\text{H}_2\text{O}_2$  were low (see in **Figure 12**). However, after  $\text{H}_2\text{O}_2$  was treated with the LY@ZnO group, the highest

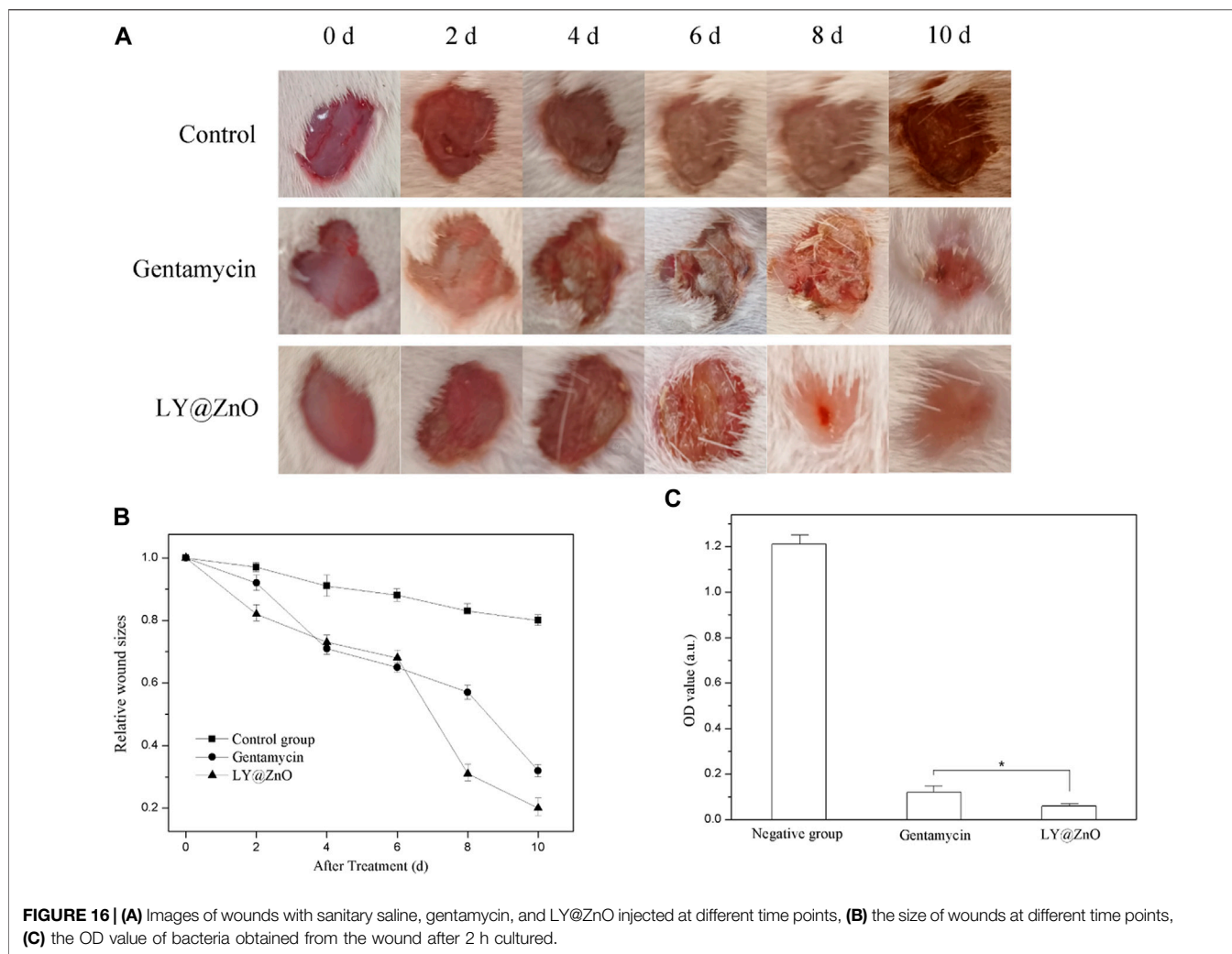




concentration of  $H_2O_2$  was observed, indicating that the LY@ZnO possessed the remarkable activity of the oxidase mimetic enzymes. Moreover, TMB is a common substrate for peroxidase, which could be reduced by the peroxidase-mimicking enzyme. **Figure 13** presents the absorbance of TMB treated with different concentrations of LY@ZnO. As shown in **Figure 13**, the absorbance showed concentration dependence as the concentration of LY@ZnO changed, meaning that LY@ZnO exhibited the activity of peroxidase-mimicking enzyme. Therefore, the generation of ROS might be due to the inherent oxidase-mimetic and peroxidase-mimetic enzyme activity of LY@ZnO.

### Biocompatibility CCK8 of the Normal Cells

Based on the LO2, BEAS-2B, CATH.a, H9C2, and MA104 cells as the cellular toxicity models, the toxicity against cells is shown in **Figure 14**. The cell viability of LO2, BEAS-2B, CATH.a, H9C2, and MA104 were 86.2%, 89.8%, 88.4%, 91.0%, and 80.7%, respectively, with the concentration of 20.0 mg/L LY@ZnO, which proved that the LY@ZnO showed low toxicity against normal cells. However, the cell viability of gentamycin was lower than that of the LY@ZnO groups at the same concentration, showing that LY@ZnO might be a safer antibacterial agent than gentamycin.



### Pathological Sections

The pathological sections of the lung, liver, spleen, kidney, and heart treated with LY@ZnO are presented in **Figure 15**. Compared with the negative group (physiological saline group), the LY@ZnO group showed no clear damage to the rat organs, indicating that LY@ZnO possessed low toxicity and excellent biocompatibility *in vivo*. These experiments displayed that LY@ZnO had a great prospect in the treatment of bacterial infection *in vivo*.

### *In vivo* Antimicrobial Properties

In our experiments, the rat skin infection model was used to estimate the treatment of LY@ZnO against the MRSA *in vivo* (see in **Figure 16**). As shown in **Figure 16A**, the infected wound healing in the negative group was poor. However, compared with the negative group, the infected wounds in the LY@ZnO were basically recovered, showing good efficacy in the treatment of the infected wounds. Furthermore, the relative wound sizes are shown in **Figure 16B**. It was found that the relative wound size of the LY@ZnO group was smaller than that of the positive

group and the negative group. These results indicated that LY@ZnO could facilitate the healing of infected wounds. Besides, the OD values of bacteria obtained from the wound are shown in **Figure 16C**. The OD values of the LY@ZnO group were lower than those of the positive and the negative groups, showing excellent therapeutic effects against infected wounds caused by bacteria *in vivo*. Therefore, the LY@ZnO possessed great potential for clinical application in treating infectious diseases, especially infections induced by multidrug-resistant bacteria.

### CONCLUSION

In conclusion, the LY@ZnO NPs were synthesized successfully by the reduction–oxidation method. After a series of antibacterial experiments tested, the high antibacterial ability against *E. coli* and *S. aureus* of LY@ZnO were proposed, which might be attributed to the synergistic effects by LY and ZnO nanoparticles. The antibacterial mechanism of LY@ZnO was discovered to induce the death of bacteria by ROS generation.

The antibacterial mechanism of LY@ZnO was discovered to induce the death of bacteria by ROS generation. The generation of ROS might be attributed to the oxidase-mimetic/peroxidase-mimetic enzyme activity of LY@ZnO. Moreover, the biological effect of the LY@ZnO *in vitro* and *in vivo* was evaluated, which showed low toxicity, excellent biocompatibility, and facilitating the healing. Our findings revealed that LY@ZnO showed fascinating prospects as an antibacterial drug, which provided clinical application in the field of wound anti-infection therapy.

## DATA AVAILABILITY STATEMENT

The original contributions presented in the study are included in the article/Supplementary Material; further inquiries can be directed to the corresponding authors.

## ETHICS STATEMENT

The animal study was reviewed and approved by the Guangdong Medical University Laboratory Animal Ethics Committee.

## REFERENCES

- Anićić, N., Vukomanović, M., Koklič, T., and Suvorov, D. (2018). MgO Antibacterial Properties: Fewer Defects in the Surface Slows the Hydrolysis Rate, Decreases the ROS Generation Potential, and Improves the Non-ROS Antimicrobial Activity of MgO (Small 26/2018). *Small* 14, 1870123. doi:10.1002/smll.201870123
- Biju, V. (2013). Chemical Modifications and Bioconjugate Reactions of Nanomaterials for Sensing, Imaging, Drug Delivery and Therapy. *Chem. Soc. Rev.* 43, 744–764. doi:10.1039/c3cs60273g
- Cao, Y., Wang, H.-J., Cao, C., Sun, Y.-Y., Yang, L., and Zhang, Y.-N. (2011). Synthesis and Anti-ultraviolet Properties of Monodisperse BSA-Conjugated Zinc Oxide Nanoparticles. *Mater. Lett.* 65, 340–342. doi:10.1016/j.matlet.2010.10.044
- Chen, S., Hao, X., Liang, X., Zhang, Q., Zhang, C., Zhou, G., et al. (2016). Inorganic Nanomaterials as Carriers for Drug Delivery. *J. Biomed. Nanotechnol.* 12, 1–27. doi:10.1166/jbn.2016.2122
- Chen, Z., Wang, Z., Ren, J., and Qu, X. (2018). Enzyme Mimicry for Combating Bacteria and Biofilms. *Acc. Chem. Res.* 51, 789–799. doi:10.1021/acs.accounts.8b00011
- Das, B. K., Verma, S. K., Das, T., Panda, P. K., Parashar, K., Suar, M., et al. (2019). Altered Electrical Properties with Controlled Copper Doping in ZnO Nanoparticles Infers Their Cytotoxicity in Macrophages by ROS Induction and Apoptosis. *Chemico-Biological Interactions* 297, 141–154. doi:10.1016/j.cbi.2018.11.004
- De Meutter, J., and Goormaghtigh, E. (2020). Searching for a Better Match between Protein Secondary Structure Definitions and Protein FTIR Spectra. *Anal. Chem.* 93, 1561–1568. doi:10.1021/acs.analchem.0c03943
- Deusenbery, C., Wang, Y., and Shukla, A. (2021). Recent Innovations in Bacterial Infection Detection and Treatment. *ACS Infect. Dis.* 7, 695–720. doi:10.1021/acscinfdis.0c00890
- Du, M., Zhao, W., Ma, R., Xu, H., Zhu, Y., Shan, C., et al. (2021). Visible-light-driven Photocatalytic Inactivation of *S. aureus* in Aqueous Environment by Hydrophilic Zinc Oxide (ZnO) Nanoparticles Based on the Interfacial Electron Transfer in *S. aureus*/ZnO Composites. *J. Hazard. Mater.* 418, 126013. doi:10.1016/j.jhazmat.2021.126013
- Eyvazi, S., Vostakolaei, M. A., Dilmaghani, A., Borumandi, O., Hejazi, M. S., Kahroba, H., et al. (2020). The Oncogenic Roles of Bacterial Infections in Development of Cancer. *Microb. Pathogenesis* 141, 104019. doi:10.1016/j.micpath.2020.104019
- Gao, X., Cui, Y., Levenson, R. M., Chung, L. W. K., and Nie, S. (2004). *In Vivo* cancer Targeting and Imaging with Semiconductor Quantum Dots. *Nat. Biotechnol.* 22, 969–976. doi:10.1038/nbt994
- Guo, L., He, N., Zhao, Y., Liu, T., and Deng, Y. (2020). Autophagy Modulated by Inorganic Nanomaterials. *Theranostics* 10, 3206–3222. doi:10.7150/thno.40414
- Guo, S., and Wang, E. (2011). Noble Metal Nanomaterials: Controllable Synthesis and Application in Fuel Cells and Analytical Sensors. *Nano Today* 6, 240–264. doi:10.1016/j.nantod.2011.04.007
- Gutha, Y., Pathak, J. L., Zhang, W., Zhang, Y., and Jiao, X. (2017). Antibacterial and Wound Healing Properties of Chitosan/poly(vinyl Alcohol)/zinc Oxide Beads (CS/PVA/ZnO). *Int. J. Biol. Macromolecules* 103, 234–241. doi:10.1016/j.ijbiomac.2017.05.020
- Hajipour, M. J., Fromm, K. M., Akbar Ashkarran, A., Jimenez de Aberasturi, D. A., Larramendi, I. R. d., Rojo, T., et al. (2012). Antibacterial Properties of Nanoparticles. *Trends Biotechnol.* 30, 499–511. doi:10.1016/j.tibtech.2012.06.004
- Han, L., Zhang, X.-Y., Wang, Y.-L., Li, X., Yang, X.-H., Huang, M., et al. (2017). Redox-responsive Theranostic Nanoplatfoms Based on Inorganic Nanomaterials. *J. Controlled Release* 259, 40–52. doi:10.1016/j.jconrel.2017.03.018
- Jiang, J., Li, Y., Liu, J., Huang, X., Yuan, C., and Lou, X. W. D. (2012). Recent Advances in Metal Oxide-Based Electrode Architecture Design for Electrochemical Energy Storage. *Adv. Mater.* 24, 5166–5180. doi:10.1002/adma.201202146
- Lan, S., Sheng, X., Lu, Y., Li, C., Zhao, S., and Liu, N. (2018). Modification of Antibacterial ZnO Nanorods with CeO<sub>2</sub> Nanoparticles: Role of CeO<sub>2</sub> in Impacting Morphology and Antibacterial Activity. *Colloid Interf. Sci. Commun.* 26, 32–38. doi:10.1016/j.colcom.2018.08.002
- Mei, L., Zhu, S., Liu, Y., Yin, W., Gu, Z., and Zhao, Y. (2021). An Overview of the Use of Nanozymes in Antibacterial Applications. *Chem. Eng. J.* 418, 129431. doi:10.1016/j.cej.2021.129431
- Pinegin, B., Vorobjeva, N., Pashenkov, M., and Chernyak, B. (2017). The Role of Mitochondrial ROS in Antibacterial Immunity. *J. Cell Physiol* 233, 3745–3754. doi:10.1002/jcp.26117

## AUTHOR CONTRIBUTIONS

KY and DW contributed to the conception and design of the study. KY and XL organized the database. KY, JS, and WL performed the statistical analysis. KY, KL, and HL wrote the first draft of the manuscript. KY, ZC, and CL wrote sections of the manuscript. All authors contributed to manuscript revision, read, and approved the submitted version.

## FUNDING

The authors would like acknowledge the grants from the National Natural Science Foundation of Guangdong Province (No. 2019A1515110017 and No. 2018A030307003), Science and Technology Foundation of Chinese Medicine Department of Guangdong Province (No.20212100), Science and Technology Foundation of Guangdong Medical University (No. GDMUZ2020006), Dongguan Science and Technology Specialists Project (No. 20201800500062), Guangdong Medical University Nanhai Marine Biomedical Resources R&D Public Service Platform Open Fund Project (No. 2HC18013 and No. 2HC18016), and Medical Science and Technology Development Foundation of Guangdong Province (No. A2016355).

- Popescu, T., Matei, C. O., Vlaicu, I. D., Tivig, I., Kuncser, A. C., Stefan, M., et al. (2020). Influence of Surfactant-Tailored Mn-Doped ZnO Nanoparticles on ROS Production and DNA Damage Induced in Murine Fibroblast Cells. *Sci. Rep.* 10 (1), 18062. doi:10.1038/s41598-020-74816-0
- Qi, K., Cheng, B., Yu, J., and Ho, W. (2017). Review on the Improvement of the Photocatalytic and Antibacterial Activities of ZnO. *J. Alloys Comp.* 727, 792–820. doi:10.1016/j.jallcom.2017.08.142
- Rasal, A. S., Yadav, S., Yadav, A., Kashale, A. A., Manjunatha, S. T., Altaee, A., et al. (2021). Carbon Quantum Dots for Energy Applications: A Review. *ACS Appl. Nano Mater.* 4, 6515–6541. doi:10.1021/acsnano.1c01372
- Shang, J., Sun, Y., Zhang, T., Liu, Z., and Zhang, H. (2019). Enhanced Antibacterial Activity of Ag Nanoparticle-Decorated ZnO Nanorod Arrays. *J. Nanomater.* 2019, 1–7. doi:10.1155/2019/3281802
- Silvestre, C., Duraccio, D., and Cimmino, S. (2011). Food Packaging Based on Polymer Nanomaterials. *Prog. Polym. Sci.* 36, 1766–1782. doi:10.1016/j.progpolymsci.2011.02.003
- Tang, G., He, J., Liu, J., Yan, X., and Fan, K. (2021). Nanozyme for Tumor Therapy: Surface Modification Matters. *Exploration* 1, 75–89. doi:10.1002/exp.20210005
- Tao, Y., Ju, E., Ren, J., and Qu, X. (2014). Bifunctionalized Mesoporous Silica-Supported Gold Nanoparticles: Intrinsic Oxidase and Peroxidase Catalytic Activities for Antibacterial Applications. *Adv. Mater.* 27, 1097–1104. doi:10.1002/adma.201405105
- Theuretzbacher, U., Bush, K., Harbarth, S., Paul, M., Rex, J. H., Tacconelli, E., et al. (2020). Critical Analysis of Antibacterial Agents in Clinical Development. *Nat. Rev. Microbiol.* 18, 286–298. doi:10.1038/s41579-020-0340-0
- Wang, B., Ruan, T., Chen, Y., Jin, F., Peng, L., Zhou, Y., et al. (2020). Graphene-based Composites for Electrochemical Energy Storage. *Energ. Storage Mater.* 24, 22–51. doi:10.1016/j.ensm.2019.08.004
- Wang, L., Hortelão, A. C., Huang, X., and Sánchez, S. (2019). Lipase-Powered Mesoporous Silica Nanomotors for Triglyceride Degradation. *Angew. Chem. Int. Ed.* 58, 7992–7996. doi:10.1002/anie.201900697
- Wang, L., Lin, Y., Zhou, Y., Xie, H., Song, J., Li, M., et al. (2019). Autonomic Behaviors in Lipase-Active Oil Droplets. *Angew. Chem. Int. Ed.* 58, 1067–1071. doi:10.1002/anie.201812111
- Wang, L., Marciello, M., Estévez-Gay, M., Soto Rodriguez, P. E. D., Luengo Morato, Y., Iglesias-Fernández, J., et al. (2020). Enzyme Conformation Influences the Performance of Lipase-powered Nanomotors. *Angew. Chem. Int. Ed.* 59, 21080–21087. doi:10.1002/anie.202008339
- Wang, M., Li, M., Wang, Y., Shao, Y., Zhu, Y., and Yang, S. (2021). Efficient Antibacterial Activity of Hydroxyapatite through ROS Generation Motivated by Trace Mn(III) Coupled H Vacancies. *J. Mater. Chem. B.* 9, 3401–3411. doi:10.1039/d1tb00098e
- Wang, X., Zhong, X., Li, J., Liu, Z., and Cheng, L. (2021). Inorganic Nanomaterials with Rapid Clearance for Biomedical Applications. *Chem. Soc. Rev.* 50, 8669–8742. doi:10.1039/d0cs00461h
- Wei, H., Gao, L., Fan, K., Liu, J., He, J., Qu, X., et al. (2021). Nanozymes: A clear Definition with Fuzzy Edges. *Nano Today* 40, 101269. doi:10.1016/j.nantod.2021.101269
- Wu, T., Wu, C., Fu, S., Wang, L., Yuan, C., Chen, S., et al. (2017). Integration of Lysozyme into Chitosan Nanoparticles for Improving Antibacterial Activity. *Carbohydr. Polym.* 155, 192–200. doi:10.1016/j.carbpol.2016.08.076
- Xiao, L., Ni, W., Zhao, X., Guo, Y., Li, X., Wang, F., et al. (2019). A Moisture Balanced Antibacterial Dressing Loaded with Lysozyme Possesses Antibacterial Activity and Promotes Wound Healing. *Soft Matter* 17, 3162–3173. doi:10.1039/d0sm02245d
- Xin, Q., Shah, H., Nawaz, A., Xie, W., Akram, M. Z., Batool, A., et al. (2018). Antibacterial Carbon-Based Nanomaterials. *Adv. Mater.* 31, 1804838. doi:10.1002/adma.201804838
- Ye, Y., Klimchuk, S., Shang, M., and Niu, J. (2019). Improved Antibacterial Performance Using Hydrogel-Immobilized Lysozyme as a Catalyst in Water. *RSC Adv.* 9, 20169–20173. doi:10.1039/c9ra02464f
- Yin, W., Yu, J., Lv, F., Yan, L., Zheng, L. R., Gu, Z., et al. (2016). Functionalized Nano-MoS<sub>2</sub> with Peroxidase Catalytic and Near-Infrared Photothermal Activities for Safe and Synergetic Wound Antibacterial Applications. *ACS Nano* 10, 11000–11011. doi:10.1021/acsnano.6b05810
- Zhang, R., Yan, X., and Fan, K. (2021). Nanozymes Inspired by Natural Enzymes. *Acc. Mater. Res.* 2 (7), 534–547. doi:10.1021/accountsmr.1c00074
- Zhao, H., Zhang, R., Yan, X., and Fan, K. (2021). Superoxide Dismutase Nanozymes: an Emerging star for Anti-oxidation. *J. Mater. Chem. B.* 9, 6939–6957. doi:10.1039/d1tb00720c
- Zhou, Z.-Y., Tian, N., Li, J.-T., Broadwell, I., and Sun, S.-G. (2011). Nanomaterials of High Surface Energy with Exceptional Properties in Catalysis and Energy Storage. *Chem. Soc. Rev.* 40, 4167–4185. doi:10.1039/c0cs00176g

**Conflict of Interest:** The authors declare that the research was conducted in the absence of any commercial or financial relationships that could be construed as a potential conflict of interest.

**Publisher's Note:** All claims expressed in this article are solely those of the authors and do not necessarily represent those of their affiliated organizations, or those of the publisher, the editors and the reviewers. Any product that may be evaluated in this article, or claim that may be made by its manufacturer, is not guaranteed or endorsed by the publisher.

Copyright © 2021 Yuan, Liu, Shi, Liu, Lu, Wu, Chen and Lu. This is an open-access article distributed under the terms of the Creative Commons Attribution License (CC BY). The use, distribution or reproduction in other forums is permitted, provided the original author(s) and the copyright owner(s) are credited and that the original publication in this journal is cited, in accordance with accepted academic practice. No use, distribution or reproduction is permitted which does not comply with these terms.